Near-ultraviolet absorption spectra and crystal-field analysis of Gd^{3+} in $Na_3[Gd(C_4H_4O_5)_3]\cdot 2NaClO_4\cdot 6H_2O$

Eileen M. Stephens
Department of Surgery, School of Medicine, University of Virginia, Charlottesville, Virginia 22908

David H. Metcalf, Mary T. Berry, and F. S. Richardson*
Department of Chemistry, University of Virginia, Charlottesville, Virginia 22901
(Received 27 August 1990)

Optical absorption spectra between 32 000 and 41 000 cm^{-1} are reported for Gd^{3+} in trigonal $Na_3[Gd(oxydiacetate)_3]\cdot 2NaClO_4\cdot 6H_2O$ at temperatures between 10 and 298 K. Fifty-eight of the 63 crystal-field levels split out of the ^6P_J($J=7/2$, 5/2, and 3/2), ^6I_J($J=7/2$, 9/2, 17/2, 11/2, 15/2, and 13/2), and ^6D_J($J=9/2$, 1/2, 7/2, 3/2, and 5/2) multiplets of the Gd^{3+} $4f^7$ electronic configuration are located and assigned from the low-temperature spectra, and these energy levels are analyzed in terms of a parametrized Hamiltonian that reflects D_3 site symmetry at the Gd^{3+} ions. Parametric fits of calculated to empirical-energy-level data yield a rms deviation of 6.3 cm^{-1} (between calculated and observed energies). Eigenvectors of the parametrized Hamiltonian are used in calculations of oscillator strengths for all transitions that originate from the $^8S_{7/2}$ (ground) multiplet and terminate on crystal-field levels of the ^6P_J, ^6I_J, and ^6D_J multiplet manifolds. Spectra simulations based on these calculated oscillator strengths are presented, and comparisons between the simulated spectra and experimentally observed spectra show excellent agreement with respect to intensity distributions both *within* and *between* the various multiplet-to-multiplet transition manifolds. Variable-temperature absorption measurements carried out between 10 and 298 K showed only very small changes in J-multiplet baricenter energies, crystal-field-splitting energies (within J-multiplet manifolds), and transition intensity distributions. Disparities between the energy-level structure deduced in the present study and that proposed in another recently published study of $Na_3[Gd(oxydiacetate)_3]\cdot 2NaClO_4\cdot 6H_2O$ [Phys. Rev. B **41**, 10 911 (1990)] are discussed. This previous study of Kundu, Banerjee, and Chowdhury was based on two-photon luminescence excitation measurements that have special significance for elucidating two-photon-absorption intensity mechanisms of $4f$-$4f$ transitions in noncentrosymmetric lanthanide systems. However, the energy-level structure deduced from those measurements differs from that deduced from the one-photon-absorption results reported in the present study.

I. INTRODUCTION

The isomorphous series of compounds $Na_3[M(C_4H_4O_5)_3]\cdot 2NaClO_4\cdot 6H_2O$ formed by trivalent lanthanide ions (M^{3+}) and oxydiacetate dianions ($C_4H_4O_5^{2-} \equiv {}^-OOCCH_2OCH_2COO^-$) in aqueous solution with perchloric acid have received considerable attention as model systems for investigating ligand-field effects on lanthanide $4f^N$ electronic state structure and optical properties.[1–45] Optical-quality, single crystals of these compounds are readily grown from aqueous solution, and at room temperature the crystals belong to the space group $R32$ (Refs. 46–49). The M^{3+} ions are located at sites with D_3 symmetry, and each M^{3+} ion is coordinated to three oxydiacetate (ODA) ligands to form a tris-terdentate $M(ODA)_3^{3-}$ complex of trigonal-dihedral (D_3) point-group symmetry. The MO_9 coordination cluster in these complexes forms a slightly distorted tricapped trigonal prism polyhedron (of D_3 symmetry), with the top and bottom triangles defined by carboxylate oxygen atoms and the capping positions (on normals to the rectangular faces) occupied by ether oxygen atoms. The backbone of each bicyclic $M(ODA)$ chelate ring system is nearly planar and stretches diagonally across a rectangular face of the MO_9 trigonal prism structure. The chelate rings contain highly anisotropic electronic charge distributions, and their interactions with the lanthanide $4f$ electrons produce effects not ordinarily seen in structurally simpler systems. The trigonal $Na_3[M(ODA)_3]\cdot 2NaClO_4\cdot 6H_2O$ systems have proved to be extraordinarily useful model systems for investigating lanthanide $4f^N$ electronic state structure and $4f$-$4f$ optical transition processes in a relatively complex, but structurally well-defined, ligand environment.

Among the $Na_3[M(ODA)_3]\cdot 2NaClO_4\cdot 6H_2O$ systems examined to date, the neodymium,[35,39,40,50] samarium,[27–30,50] europium,[33,34] holmium,[38,43,44] and erbium[36,51] members of the series have been most thoroughly characterized with respect to $4f^N$ electronic state structure and optical properties. A considerable amount of spectroscopic data has been reported for other members of the series, but detailed analyses of these data remain incomplete. In this paper we report optical-absorption spectra and a crystal-field energy-level analysis for Gd^{3+} in trigonal $Na_3[Gd(ODA)_3]\cdot 2NaClO_4\cdot 6H_2O$ (referred to hereafter as GdODA). Chowdhury and co-workers have

reported several spectroscopic studies of the GdODA system, the most recent being an investigation of the two-photon luminescence excitation spectra of GdODA crystals at room temperature.[42] Chowdhury's one-photon-absorption and circular dichroism spectra were not sufficiently well resolved to permit detailed assignments and analyses of the $4f^7$ (Gd^{3+}) crystal-field energy levels, but the two-photon luminescence excitation spectra did reveal sufficient structure to permit many crystal-field energy-level assignments to be made. Among the 63 crystal-field levels lying between 32 000 and 41 000 cm^{-1}, Chowdhury and co-workers located and assigned 33 of the levels from their two-photon luminescence excitation results, and they analyzed their assigned levels in terms of a model crystal-field Hamiltonian (of D_3 symmetry).[42] They performed calculated to experimentally-observed-energy-level fits and achieved reasonably good agreement between calculated and observed crystal-field splittings within several J-multiplet manifolds; however, the overall quality of their energy-level fits suffered from generally poor agreement between calculated and observed J-multiplet baricenter energies. The two-photon-absorption intensity data measured by Chowdhury and co-workers was analyzed in terms of $4f^7$ electronic state vectors obtained as eigenvectors of the parametrized Hamiltonian derived from their energy-level fits.

We have performed one-photon-absorption measurements on GdODA crystals at temperatures between 10 and 298 K, and have located and assigned 58 of the 63 levels lying between 32 000 and 41 000 cm^{-1}. These levels span the 14 lowest-energy J-multiplet manifolds of ^6P, ^6I, and ^6D $4f^7$ SL-term parentage. Approximately two-thirds of the assigned levels could be located from resolved transitions in the 298 K absorption spectra, but locations for the full complement of assigned levels could only be obtained from absorption spectra recorded at sample temperatures below 150 K. The GdODA crystals retain macroscopic uniaxial symmetry over the entire 298–10 K temperature range represented in our absorption measurements, and this conforms with the macroscopic symmetry properties observed for other MODA systems. However, there is evidence that at least several of these systems undergo low-temperature structural phase transitions in which the crystal space group changes from $R32$ to $P321$, and the lanthanide site symmetry is reduced from D_3 to C_2 (due to movement of the Na^+ ions off threefold axes).[11,14,35,45] This type of structural change is relatively easy to detect in the $4f$-$4f$ optical spectra of MODA systems with an *even* number of $4f$ electrons, because in these cases the crystal-field levels that are doubly degenerate in D_3 symmetry generally split into resolvable nondegenerate components when the lanthanide site symmetry is reduced to C_2 (Refs. 14 and 43). However, for systems with an *odd* number of $4f$ electrons, all the crystal-field levels are Kramer's doublets and their degeneracy is not removed by a lowering of the lanthanide site symmetry. Comparisons between the room-temperature (298 K) and low-temperature (down to 10 K) absorption spectra obtained for GdODA crystals indicate that crystal-field splittings within J-multiplet manifolds *and* relative line strengths of transitions occurring within ground-multiplet to excited-multiplet transition manifolds are essentially invariant to temperature. Except for resolution, the only apparent differences between the room-temperature and low-temperature spectra are small *red shifts* ($\approx$5–10 cm^{-1}) observed within several transition manifolds when the sample temperature is lowered from 298 to 10 K.

Chowdhury's energy-level assignments and analyses span *nine* of the 14 excited multiplet manifolds examined in the present study. These nine multiplets are ^6P_J(J=7/2, 5/2, and 3/2), ^6I_J(J=7/2 and 11/2), and ^6D_J(J=9/2, 7/2, 3/2, and 5/2). Comparisons between his energy-level data and ours over these multiplet manifolds reveal both similarities *and* significant discrepancies, and his calculated-to empirical-energy-level fits yield atomic and crystal-field Hamiltonian parameters that bear little resemblance to the ones we obtain. In general, our energy-level data sets are in good agreement with respect to observed splittings between crystal-field levels *within* various J-multiplet manifolds, although our assignments of D_3 double-group irreps (E' or E'') to crystal-field levels differ within several multiplet manifolds (*vide infra*). The largest differences between the respective data sets are found in the multiplet baricenter energies. These differences range from 24 cm^{-1} (for $^6I_{7/2}$) to 107 cm^{-1} (for $^6D_{9/2}$), and, *on average,* our baricenters are 50–60 cm^{-1} *lower* than those reported by Chowdhury. We will defer further comment on these differences until later in the paper, but we point out here that they can have a dramatic effect on the Hamiltonian parameter values deduced from energy-level fits, and accurate parametrization of the Hamiltonian is absolutely crucial for calculating state vectors that are suitable for use in $4f$-$4f$ transition intensity analyses. In the present study, we focus on a detailed characterization of the $4f^N$ energy-level structure and *one-photon*-absorption spectra of GdODA between 32 000 and 41 000 cm^{-1}, and we propose a parametrized model Hamiltonian whose eigenvalues and eigenvectors give a good account of the experimentally observed energy-level locations and one-photon-absorption intensities. It is likely that this Hamiltonian and its eigenvectors will also be useful in refined analyses of the two-photon-absorption (TPA) intensity data reported by Kundu, Banerjee, and Chowdhury,[42] but these analyses lie outside the scope of the present study.

II. EXPERIMENT

Single crystals of $Na_3[Gd(ODA)_3]\cdot 2NaClO_4\cdot 6H_2O$ were grown from an aqueous solution following the methods of Albertsson.[46,47] Damp Whatman glass-microfiber filter paper was used to polish crystals to a thickness and shape suitable for optical measurements. Variable-temperature measurements between 10 and 298 K were carried out with the crystal sample mounted at the cold station in the sample compartment of a CTI-Cryogenics closed-cycle helium refrigerator-cryostat. The crystal was mounted on a one-piece copper mount using crycon grease and indium foil, and the copper mount was attached to the cold head of the refrigerator,

with strips of indium providing a thermally conductive interface. Cold-head temperature was controlled using a Lake Shores temperature controller (model DRC-70), and it could be varied between approximately 10 and 298 K.

Absorption spectra were recorded on a lab-built, high-resolution spectrophotometer normally used for emission and Raman spectroscopic measurements. Broad-band radiation from a xenon arc lamp (500 W, PTI A5000 housing) was passed through the crystal sample, and the transmitted radiation was then dispersed with a 0.75-m Spex double-grating monochromator in which the gratings are blazed for first-order diffraction at 500 nm. The *second-order* output of the monochromator was scanned to obtain an optical transmission spectrum of the GdODA crystal sample between 315 and 240 nm. Transmission intensity was measured using an EMI-9558 photomultiplier tube and associated lab-built photon-counting electronics. The transmission spectrum was converted to an absorbance spectrum by correcting for the arc-lamp output profile *and* for the second-order dispersion characteristics of the monochromator. Absorption spectra were also recorded with a Cary model 17D spectrophotometer, but the spectral resolution obtainable with this instrument (approximately $\Delta\lambda=0.1$ nm) is at least an order of magnitude less than that achievable with the instrumentation and measurement techniques described above.

All absorption measurements were carried out on crystals aligned with their *unique*, crystallographic c axis parallel to the direction of light propagation (i.e., the *axial* optical configuration). Crystals of two different thicknesses (optical path lengths) were employed, and these thicknesses are reported in the captions of figures that show absorption spectra with absorbance scales (*vide infra*).

III. CALCULATIONS AND DATA ANALYSIS

A. Energy levels

The ground multiplet of the Gd^{3+} $4f^7$ electronic configuration is $^8S_{7/2}$, and the excited J multiplets lying between 32 000 and 41 000 cm^{-1} are ^6P_J($J=7/2$, 5/2, and 3/2), ^6I_J($J=7/2$, 9/2, 17/2, 11/2, 15/2, and 13/2), and ^6D_J($J=9/2$, 1/2, 7/2, 3/2, and 5/2). In D_3 crystal-field symmetry, each J-multiplet may be characterized in terms of $(2J+1)/2$ crystal-field levels, and each crystal-field level is a Kramer's doublet whose degenerate JM_J components may be defined to transform as either an E' or E'' irreducible representation (*irrep*) in the D_3 double-group. The ground multiplet ($^8S_{7/2}$) contains three E' crystal-field levels ($M_J=\pm1/2$, $\pm5/2$, and $\pm7/2$) and one E'' level ($M_J=\pm3/2$), but the energy differences between these levels are too small to be detected in our optical experiments. The ^6P_J, ^6I_J, and ^6D_J excited multiplets (noted above) contain a combined total of 63 crystal-field levels, and, in most cases, the splittings between these levels are sufficiently large to be detected in optical-absorption spectra (based on transitions originating within the $^8S_{7/2}$ ground multiplet manifold). Therefore, all of the lines observed in our absorption spectra between 32 000 and 41 000 cm^{-1} are assigned to transitions that *originate* from the essentially eightfold degenerate $^8S_{7/2}$ multiplet manifold and *terminate* on doubly-degenerate crystal-field levels split out of the ^6P_J, ^6I_J, and ^6D_J multiplets. For the *axial* absorption experiments reported in this work, the $E''\rightarrow E''$ crystal-field transitions are electric- *and* magnetic-dipole forbidden, but the $E'\rightarrow E'$, $E'\rightarrow E''$, and $E''\rightarrow E'$ transitions are electric- *and* magnetic-dipole allowed. Therefore, since the $^8S_{7/2}$ ground multiplet manifold contains both E' levels and an E'' level, *all* transitions to crystal-field levels of the excited multiplets can have some symmetry-allowed electric- and/or magnetic-dipole character.

The $4f^7$ energy-level structure of Gd^{3+} in GdODA was analyzed in terms of a model Hamiltonian that may be written as

$$\hat{H}=\hat{H}_a+\hat{H}^{+}_{\rm cf}\ , \tag{1}$$

where $\hat{H}_a$ is defined to incorporate the isotropic parts of $\hat{H}$ (including the spherically symmetric part of the $4f$-electron–crystal-field interactions), and $\hat{H}^{+}_{\rm cf}$ is defined to represent the nonspherically symmetric components of the *even-parity* crystal field. We refer to $\hat{H}_a$ as the *atomic* Hamiltonian and call $\hat{H}^{+}_{\rm cf}$ the *crystal-field* Hamiltonian.

In our model, the $\hat{H}_a$ operator is defined by

$$\hat{H}_a=E_{\rm av}+\sum_k F^k\hat{f}_k+\alpha\hat{L}(\hat{L}+1)+\beta\hat{G}(G_2)+\gamma\hat{G}(R_7)+\sum_i T^i\hat{t}_i+\zeta_{\rm s.o.}\hat{A}_{\rm s.o.}+\sum_k P^k\hat{p}_k+\sum_j M^j\hat{m}_j\ , \tag{2}$$

where $k=2,4,6$; $i=2,3,4,6,7,8$; $j=0,2,4$; and the operators ($\hat{o}$) and their associated parameters are written according to conventional notation *and* meaning (with respect to the interactions they represent).[52,53] We define the crystal-field Hamiltonian as

$$\hat{H}^{+}_{\rm cf}=\sum_{k,m}\sum_i(B_{km}+b_{km}\hat{\mathbf{S}}\cdot\hat{\mathbf{s}}_i)\hat{u}_{km}(i)\ , \tag{3}$$

where i labels the $4f$ electrons; $\hat{u}_{km}(i)$ is a one-electron unit-tensor operator; $\hat{\mathbf{S}}$ and $\hat{\mathbf{s}}_i$ denote total spin and one-electron spin operators, respectively; B_{km} denotes a standard (one-electron) crystal-field interaction parameter; and b_{km} denotes a *spin-correlated crystal-field* parameter.[54,55] In D_3 symmetry, $\hat{H}^{+}_{\rm cf}$ may be defined in terms of six B_{km} parameters and six b_{km} parameters: $(k,m)=(2,0)$, (4,0), (4,3), (6,0), (6,3), and (6,6). Each parameter may be chosen to be pure *real*, so our model crystal-field Hamiltonian (defined to have D_3 symmetry) contains a total of 12 independent parameters.

The atomic Hamiltonian, defined by expression (2), contains 20 parameters (including $E_{\rm av}$), and the crystal-field Hamiltonian, defined by expression (3) and assuming D_3 symmetry, contains 12 parameters. The *complete* $\hat{H}_a$ operator was used in all of our energy-level calculations, although not all of the 20 parameters contained in this operator were used in performing parametric fits of calculated- to experimental-energy-levels data (*vide infra*). Calculations were carried out both *with* and *without* inclusion of the spin-correlated crystal-field

(SCCF) terms in $\hat{H}_{\rm cf}^{+}$. The SCCF terms represent some (partial) consideration of electron-correlation effects in the $4f$-electron–crystal-field interactions, and recent work by Newman, Reid, Richardson, and coworkers[54–62] suggests that these effects may sometimes have a non-negligible influence on the $4f^N$ energy-level structures of lanthanide systems. Energy-level calculations were performed in two steps. The atomic Hamiltonian was first diagonalized within the complete Russell-Saunders basis set of the $4f^7$ configuration, and the eigenvectors obtained from this calculation were then used to construct a suitably truncated intermediate-coupling $4f^7[SL]JM_J$ basis within which the *total* (atomic plus crystal-field) Hamiltonian was diagonalized. The latter basis set included all JM_J states (188) derived from $[SL]J$ multiplets with energies between 0 and 52 000 $\rm cm^{-1}$ (a total of 21 multiplets). The highest experimentally characterized energy level included in our parametric data fits was located at 40 861 $\rm cm^{-1}$.

B. Transition line strengths and spectra simulations

Electric and magnetic dipole strengths were calculated for all transitions originating from crystal-field levels of the $^8S_{7/2}$ multiplet and terminating on crystal-field levels of the ^6P_J, ^6I_J, and ^6D_J multiplets (a total of 252 transitions). For a transition between crystal-field levels A (initial) and B (final), the electric and magnetic dipole strengths are defined according to

$$D_{AB}^{(e)}=\left|\sum_a\sum_b\sum_q\langle Aa|\mu_q|Bb\rangle\right|^2, \tag{4}$$

$$D_{AB}^{(m)}=\left|\sum_a\sum_b\sum_q\langle Aa|m_q|Bb\rangle\right|^2, \tag{5}$$

where the summations are over the degenerate components of levels A and B and over the spherical components ($q=0,\pm1$) of the electric (μ_q) and magnetic (m_q) dipole moment operators.

Evaluation of expressions (4) and (5) requires state vectors for levels A and B. We choose these state vectors to be eigenvectors of the model Hamiltonian defined by Eqs. (1)–(3), and they are constructed entirely within the $\{SLJM_J\}$ basis of the Gd^{3+} $4f^7$ electronic configuration. Defined in this way, the state vectors are eigenvectors of the *even-parity* crystal-field Hamiltonian ($\hat{H}_{\rm cf}^{+}$), and they transform identically under a coordinate inversion operation. The magnetic-dipole operator in expression (5) has *even* parity, and it acts only on the nonradially dependent parts of the state vectors (which we shall denote by Ψ_{Aa} and Ψ_{Bb}). Therefore, knowing Ψ_{Aa} and Ψ_{Bb} (expressed in a $\{SLJM_J\}$ basis), evaluation of expression (5) is straightforward. On the other hand, the electric-dipole operator in expression (4) has *odd* parity, and the matrix elements in this expression will vanish when evaluated over Ψ_{Aa} and Ψ_{Bb}.

The *actual* state vectors of the system have *mixed* parity, reflecting the D_3 symmetry of the Gd^{3+} sites, and this mixed parity is essential to electric-dipole transition processes. However, in evaluating expression (4) we shall retain the state vectors described above (denoted by Ψ_{Aa} and Ψ_{Bb}), and redefine the electric-dipole operator so that it operates entirely *within* the $4f^7$ configuration. Following Reid and Richardson,[63,64] we express this "effective" electric-dipole moment operator as

$$\mu_q^{\rm eff}=-e(-1)^q\sum_{\lambda,t,p}A_{tp}^{\lambda}\sum_l\langle\lambda l,1-q|tp\rangle U_l^{\lambda}, \tag{6}$$

where $\lambda=2,4,6$; $t=\lambda,\lambda\pm1$; $p=0,\pm1,\ldots,\pm t$; $l=q+p$; U_l^{λ} is an intraconfigurational unit-tensor operator; and the A_{tp}^{λ} are parameters that contain structural and mechanistic details regarding interactions of the odd-parity crystal-field *and* the electric-dipolar radiation field with the $4f$ electrons of the systems. We note that $\mu_q^{\rm eff}$ has even parity with respect to $4f$-electron coordinates, and it operates only on the nonradial parts of the $4f^7$ state functions. If $\mu_q^{\rm eff}$ is substituted for μ_q in expression (4), the q-polarized component of the electric-dipole strength may be written as

$$D_{AB,q}^{(e)}=e^2\left|\sum_{\lambda,t,p}A_{tp}^{\lambda}\sum_l\langle\lambda l,1-q|tp\rangle(-1)^q\times\sum_{a,b}\langle\Psi_{Aa}|U_l^{\lambda}|\Psi_{Bb}\rangle\right|^2. \tag{7}$$

The $\{A_{tp}^{\lambda}\}$ parameter set must reflect the site symmetry of the lanthanide ions, and this places restrictions on the permissible pairs of (t,p) values for each value of λ.[63,64] In the case of D_3 site symmetry, the permissible (λ,t,p) combinations are (2,2,0), (2,3,±3), (4,3,±3), (4,4,0), (4,4,±3), (4,5,±3), (6,5,±3), (6,6,0), (6,6,±3), (6,6,±6), (6,7,±3), and (6,7,±6). However, we also have the relationship $(A_{tp}^{\lambda})^*=(-1)^{t+p+1}A_{t-p}^{\lambda}$, and the $\{A_{tp}^{\lambda}\}$ set contains just 12 *independent* parameters in D_3 symmetry. A subset of the A_{tp}^{λ} parameters can be related to the so-called Judd-Ofelt-Axe parametrization scheme for f-f electric-dipole intensities[65–67] according to

$$A_{tp}^{\lambda}=-(2\lambda+1)(2t+1)^{-1/2}A_{tp}\Xi(t,\lambda), \tag{8}$$

where $A_{tp}\Xi(t,\lambda)$ denotes a Judd-Ofelt-Axe intensity parameter and t is restricted to values of $\lambda\pm1$. The $t=\lambda$ members of the $\{A_{tp}^{\lambda}\}$ parameter set have no counterparts in the Judd-Ofelt-Axe intensity parametrization scheme.

In the *axial* (α) absorption experiments performed in this study, light propagates along the unique (optic) axis of the crystal, and this axis is parallel to the trigonal (C_3) symmetry axes of the $Gd(ODA)_3^{3-}$ complexes. We also define the $q=0$ component of the electric and magnetic dipole moment operators to be parallel to this axis. The oscillator strengths of transitions observed in the axial absorption experiments may be expressed as

$$f_{AB}(\alpha)=(8\pi^2m_ec/he^2)\bar{\nu}_{AB}(1/2g_A)\times\sum_q q^2[\chi'_{\alpha}D_{AB,q}^{(m)}+\chi_{\alpha}D_{AB,q}^{(e)}], \tag{9}$$

where m_e denotes electron mass, c is the speed of light, e is the elementary charge, h is the Planck constant, $\bar{\nu}_{AB}$

denotes transition frequency (expressed in wave numbers), g_A denotes the degeneracy of the initial level (A), $D^{(e)}_{AB,q}$ and $D^{(m)}_{AB,q}$ are the q-polarized components of the electric and magnetic dipole strengths, and χ_α and χ'_α are correction factors for bulk sample refractivity effects on light propagating along the optic axis of the crystal sample. If $\bar{\nu}_{AB}$ is expressed in reciprocal centimeters (cm^{-1}), the dipole strengths are expressed in units of $esu^2\,cm^2$, and $D^{(e)}_{AB,q}$ is expressed according to Eq. (7), then Eq. (9) may be rewritten as

$$f_{AB}(\alpha)=1.411\times10^{30}(\bar{\nu}_{AB}/2g_A)\left[\chi'_\alpha\left|\sum_{a,b}\sum_q q^2\langle\Psi_{Aa}|m_q|\Psi_{Bb}\rangle\right|^2 + \chi_\alpha e^2\left|\sum_{\lambda,t,p}A^\lambda_{tp}\sum_{l,q}q^2\langle\lambda l,1-q|tp\rangle(-1)^q\sum_{a,b}\langle\Psi_{Aa}|U^\lambda_l|\Psi_{Bb}\rangle\right|^2\right]. \quad (10)$$

The m_q and U^λ_l matrix elements in Eq. (10) are readily evaluated over the crystal-field state vectors obtained from our energy-level calculations (*vide supra*), but to complete the calculation of oscillator strengths we also need values for χ'_α, χ_α, and the A^λ_{tp} parameters. In several previous studies of $4f$-$4f$ transition intensities in MODA absorption spectra, we treated χ'_α, χ_α, and the A^λ_{tp} parameters as variables in performing fits of calculated-to-empirical line-strength data. The parameter sets obtained from these semiempirical line-strength analyses proved to be quite valuable for characterizing and rationalizing intensity distributions observed within *and* between large numbers of multiplet-to-multiplet transition manifolds (Refs. 29, 30, 33, 34, 40, and 44). Quantitative line-strength data for GdODA are not sufficient to support a meaningful (or reliable) semiempirical analysis based on the 12 A^λ_{tp} parameters required in D_3 symmetry. Therefore, in the present study we used χ'_α, χ_α, and A^λ_{tp} values obtained previously[33] for EuODA in our calculations of dipole strengths and oscillator strengths. The A^λ_{tp} parameters depend on the mechanistic details of interactions between the $4f$ electrons and the odd-parity components of the ligand-field potential, *and* on the lanthanide and/or ligand state admixtures produced by these interactions.[63,64] The ligand-field interactions in EuODA and GdODA are expected to be quite similar, but there are no *a priori* reasons to expect similar electronic state mixing properties for the two systems. However, as we will show later, the $4f$-$4f$ intensity distributions observed in the one-photon-absorption spectra for GdODA are reasonably well accounted for by calculations based on the EuODA $\{A^\lambda_{tp}\}$ parameter set.

Simulated *axial* absorption spectra were calculated over the 32 000–41 000 cm^{-1} spectral range using the expression

$$A_\alpha(\bar{\nu})=2.317\times10^8 c_m d\sum_{A\rightarrow B}f_{AB}(\alpha)\rho_{AB}(\bar{\nu}), \quad (11)$$

where $A_\alpha(\bar{\nu})$ denotes decadic absorbance at wave number $\bar{\nu}$, c_m denotes the molar concentration of Gd^{3+} ions in $Na_3[Gd(ODA)_3]\cdot2NaClO_4\cdot6H_2O$ ($c_m=2.174$ mol/liter), d is the crystal thickness (in cm) along the direction of light propagation, the summation is over all transitions ($A\rightarrow B$) falling within the spectral region of interest, $f_{AB}(\alpha)$ is the oscillator strength of transition $A\rightarrow B$, calculated according to Eq. (10), and $\rho_{AB}(\bar{\nu})$ is a unit-normalized line-shape function centered at the transition frequency $\bar{\nu}_{AB}$. For all of the simulated spectra calculated in this study, Lorentzian lineshape functions were used:

$$\rho_t(\bar{\nu})=(\Delta_t/\pi)[(\bar{\nu}-\bar{\nu}_t)^2+\Delta_t^2]^{-1}, \quad (12)$$

where Δ_t denotes the line half width at half height for a transition (t) located at $\bar{\nu}_t$.

In all of our calculations of $A\rightarrow B$ transition dipole strengths and oscillator strengths, the initial level (A) corresponds to the $^8S_{7/2}$ multiplet and includes all eight M_J components of this multiplet. Therefore, the summation $\sum_a$ in Eqs. (4), (5), (7), (9), and (10) is over the eight lowest-energy eigenvectors of our model Hamiltonian.

IV. RESULTS

A. Energy levels

The energy levels located and assigned from our low-temperature-absorption spectra are listed in Table I. The levels are identified with respect to the principal $SLJM_J$ components of their eigenvectors, calculated according to the procedures described earlier in Sec. III A. The "observed" energies listed in Table I were obtained from locations of peaks in the absorption spectra, and they include the appropriate $1/\lambda$(air) to $1/\lambda$(vacuum) wavenumber corrections. The "calculated" energies are eigenvalues of the parametrized Hamiltonian defined by Eqs. (1)–(3), with the parameter values shown in Table II. Among the 26 parameters in the Hamiltonian, 13 were treated as variables in performing calculated- to empirical-energy-level fits, 11 were assigned *fixed* values (equal or close to the values reported previously for Gd^{3+} in LaF_3 or $LaCl_3$) (Refs. 53 and 61), and two (P^4 and P^6) were constrained to fixed ratios with one of the freely varying parameters (P^2). The rms deviation between the calculated and observed energies shown in Table I is 6.3 cm^{-1}.

In the calculations cited above, the spin-correlated crystal-field (SCCF) interaction terms in $\hat{H}^+_{cf}$ were neglected [i.e., the b_{km} paramaters of Eq. (3) were set equal to zero]. Additional calculations were carried out in which the SCCF interactions were included and various subsets (*or* all) of the b_{km} parameters were allowed to vary in performing data fits. These calculations did not

TABLE I. Calculated and observed energy levels for Gd^{3+} in $Na_3[Gd(ODA)_3]\cdot 2NaClO_4\cdot 6H_2O$.

				Energy/cm^{-1}		
Level No.	Multiplet[a]	$\lvert 2M_J\rvert$[a]	Γ[b]	Calculated[c]	Observed[d]	Δ[e]
1	$^8S_{7/2}$	7	E'	0.58	0	0.58
2		1	E'	0.61		
3		3	E''	0.62	0	0.62
4		5	E'	0.63		
5	$^6P_{7/2}$	1	E'	32 040	32 036	4
6		7	E'	32 054	32 044	10
7		3	E''	32 058	32 048	10
8		5	E'	32 065	32 057	8
9	$^6P_{5/2}$	5	E'	32 616	32 630	−14
10		1	E'	32 635	32 647	−12
11		3	E''	32 638	32 653	−15
12	$^6P_{3/2}$	1	E'	33 205	33 205	0
13		3	E''	33 213	33 213	0
14	$^6I_{7/2}$	1	E'	35 745	35 736	9
15		7	E'	35 788	35 786	2
16		3	E''	35 790	35 788	2
17		5	E'	35 809	35 813	−4
18	$^6I_{9/2}$	1	E'	36 093	36 089	4
19		9	E''	36 104	36 104	0
20		3	E''	36 128	36 124	4
21		5	E'	36 138	36 138	0
22		7	E'	36 147	36 146	1
23	$^6I_{17/2}$	11	E'	36 170	36 162	8
24		9	E''	36 170	36 164	6
25		7	E'	36 172	36 165	7
26		15	E''	36 181	36 176	5
27		1	E'	36 181	36 177	4
28		5	E'	36 189	36 182	7
29		7	E'	36 193		
30		9	E''	36 194	36 203	−9
31		17	E'	36 202	36 203	−1
32	$^6I_{11/2}$	1	E'	36 369	36 369	0
33		11	E'	36 382	36 384	−2
34		3	E''	36 384	36 386	−2
35		5	E'	36 410	36 406	4
36		9	E''	36 419	36 420	−1
37		7	E'	36 426	36 427	−1
38	$^6I_{15/2}$, $^6I_{13/2}$	1	E'	36 487	36 485	2
39		3	E''	36 493	36 495	−2
40		11	E'	36 506		
41		15	E''	36 507		
42		13	E'	36 511	36 509	2
43		1	E'	36 519	36 519	0
44		13	E'	36 532	36 529	3
45		3	E''	36 534		
46		7	E'	36 540	36 544	−4
47		11	E'	36 546	36 553	−7
48		9	E''	36 549	36 558	−9
49		5	E'	36 556	36 561	−5
50		7	E'	36 576	36 586	−10

TABLE I. (*Continued*).

Level No.	Multiplet[a]	$\|2M_J\|$[a]	Γ[b]	Energy/cm^{-1} Calculated[c]	Observed[d]	Δ[e]
51		5	E'	36 585	36 590	−5
52		9	E''	36 590	36 597	−7
53	$^6D_{9/2}$	7	E'	39 451	39 457	−6
54		5	E'	39 468	39 476	−8
55		3	E''	39 491	39 498	−7
56		9	E''	39 544	39 544	0
57		1	E'	39 564	39 572	−8
58	$^6D_{1/2}$	1	E'	40 428	40 428	0
59	$^6D_{7/2}$	7	E'	40 531	40 529	2
60		3	E''	40 533	40 531	2
61		1	E'	40 541	40 537	4
62		5	E'	40 549	40 543	6
63	$^6D_{3/2}$	3	E''	40 699		
64		1	E'	40 703	40 700	3
65	$^6D_{5/2}$	1	E'	40 794	40 798	−4
66		5	E'	40 857	40 853	4
67		3	E''	40 868	40 861	7

[a]Identifies the *principal* $SLJM_J$ components of the eigenvectors.
[b]Irrep label in the D_3 double group.
[c]Calculated using the Hamiltonian parameter values listed in Table II.
[d]With $1/\lambda$(air) to $1/\lambda$(vacuum) correction.
[e]Difference between calculated and observed energies.

yield improved data fits, and they were inconclusive regarding the possible importance of SCCF effects on the crystal-field energy-level structure of Gd^{3+} in $Na_3[Gd(ODA)_3]\cdot 2NaClO_4\cdot 6H_2O$. All of the calculated results presented hereafter in this paper were obtained *without* inclusion of SCCF interactions.

Table III shows a major-component analysis of the $4f^7[SL]J$ (multiplet) state vectors calculated with the atomic Hamiltonian parameters of Table II, and it also lists calculated J-multiplet baricenter energies up to 52 000 cm^{-1} and experimentally observed baricenter energies up to 41 000 cm^{-1}. Table IV shows calculated and observed crystal-field-splitting energies within nine of the 14 J-multiplet manifolds lying between 32 000 and 41 000 cm^{-1}. The splitting energies are defined as displacements of crystal-field levels from the multiplet baricenters. Note that the baricenter energies and crystal-field splitting energies from Ref. 42 are also shown (in parentheses) for comparison. The crystal-field-splitting energies determined in the present study are in good agreement with those reported in Ref. 42, but there are major differences between the multiplet baricenter energies reported here and in Ref. 42. The results reported in Ref. 42 were obtained from two-photon luminescence excitation spectra of GdODA crystals at room temperature, whereas our results were obtained from high-resolution, one-photon-absorption spectra of GdODA crystals at low temperature. We could not determine precise baricenter energies from our room-temperature spectra, but semiquantitative comparisons between our low-temperature and room-temperature spectra do nor reveal any baricenter shifts larger than 5–10 cm^{-1}.

The atomic Hamiltonian parameters determined for Gd^{3+} in GdODA, LaF_3, and $LaCl_3$ are shown in Table V, and the crystal-field parameters (B_{km}) determined for GdODA and five other LODA systems are compared in Table VI. The Hamiltonian parameter values reported in Ref. 42 (for GdODA) are also listed here for comparison: $F^2=86\,940$, $F^4=65\,231$, $F^6=43\,890$, $\alpha=27.9$, $\beta=-1509.7$, $\gamma=1400$, $\zeta_{s.o.}=1469$, $B_{20}=90$, $B_{40}=1050.4$, $B_{43}=1001.1$, $B_{60}=12.4$, $B_{63}=-400$, and $B_{66}=200$ (all values given in cm^{-1}).

B. Spectra

Low-temperature-absorption spectra measured over the $^8S_{7/2}\rightarrow{}^6P_{7/2}$, $^6P_{5/2}$, $^6P_{3/2}$, $^6I_{7/2}$, $^6I_{9/2}$, $^6I_{11/2}$, $^6D_{9/2}$, $^6D_{1/2}$, $^6D_{7/2}$, $^6D_{3/2}$, and $^6D_{5/2}$ transition regions are shown in Figs. 1–9. Simulated spectra calculated according to Eq. (11) are also shown in these figures. The linewidth parameters [Δ_t of Eq. (12)] used in the spectra simulations are given in the figure captions. In two transition regions, $^8S_{7/2}\rightarrow{}^6P_{7/2}$ and $^8S_{7/2}\rightarrow{}^6P_{5/2}$, the baricenter of the calculated multiplet-to-multiplet transition

manifold was adjusted to match the observed baricenter. However, in *all* cases the line structure in the simulated spectra reflects *calculated* splittings between crystal-field levels. The wavenumber scales in Figs. 1–9 correspond to $1/\lambda$ (air).

A survey absorption spectrum over the 242.5–312.5 nm wave length region is shown in Fig. 10, along with insets that present spectral details within the $^8S_{7/2} \rightarrow {}^6I_J(J=13/2,\ 15/2,\ 11/2)$ [inset (a)] and $^8S_{7/2} \rightarrow {}^6I_J(J=17/2,9/2)$ [inset (b)] transition regions. Variable-temperature transmission spectra are shown in Fig. 11 for the $^8S_{7/2} \rightarrow {}^6I_J(J=13/2$ and $15/2)$ transition region. This region contains transitions to 15 crystal-field levels located within a 112-cm^{-1} wave-number interval. Lowering the temperature from 298 to 10 K produces shifts of less than 8 cm^{-1} in the resolved spectral

TABLE II. Hamiltonian parameters for the $4f^7$ electronic configuration of Gd^{3+} in $Na_3[Gd(ODA)_3]\cdot 2NaClO_4\cdot 6H_2O$.

Parameter[a]	Value[b]/cm^{-1}
E_{av}	87 149(17)
F^2	84 138(68)
F^4	61 637(50)
F^6	44 633(8)
α	20.6(0.1)
β	[−600]
γ	[1500]
T^2	[300]
T^3	[42]
T^4	[62]
T^6	[−295]
T^7	[350]
T^8	[310]
$\zeta_{s.o.}$	1499(1)
M^0	[3.32]
M^2	[1.86]
M^4	[1.26]
P^2	604(1)
P^4	$0.75P^2$
P^6	$0.50P^2$
B_{20}	−87(10)
B_{40}	−952(16)
B_{43}	−845(10)
B_{60}	803(49)
B_{63}	1197(27)
B_{66}	961(13)
N[c]	60
σ[d]	6.3

[a]See Eqs. (1)–(3) in the text. The SCCF terms were *not* included in $\hat{H}_{cf}^{+}$.

[b]Determined by fitting the observed energy levels listed in Table I. Values shown in square brackets were held fixed in performing the data fits.

[c]Number of experimentally characterized energy levels included in the parametric data fits.

[d]rms deviation between calculated and observed energies (in cm^{-1}).

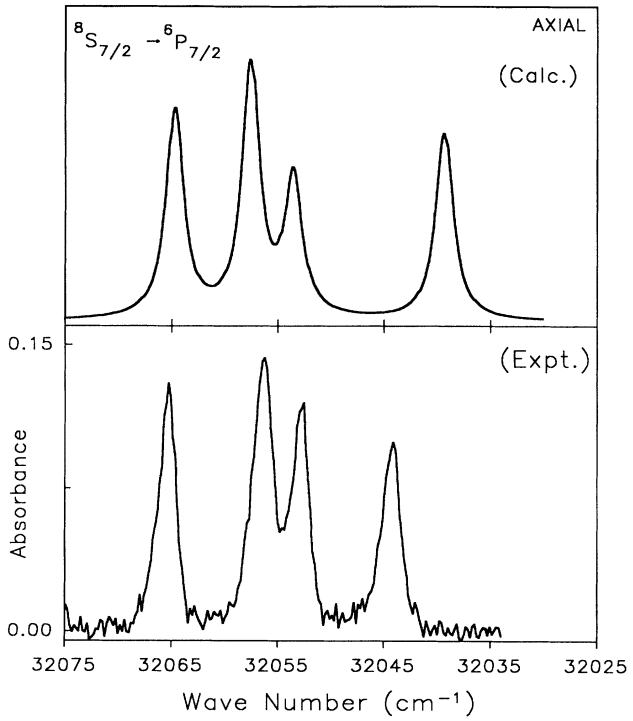

FIG. 1. Experimental and calculated absorption spectra in the $^8S_{7/2} \rightarrow {}^6P_{7/2}$ transition region. Crystal thickness, 0.175 cm; simulation linewidth parameter, $\Delta_t = 2$ cm^{-1}.

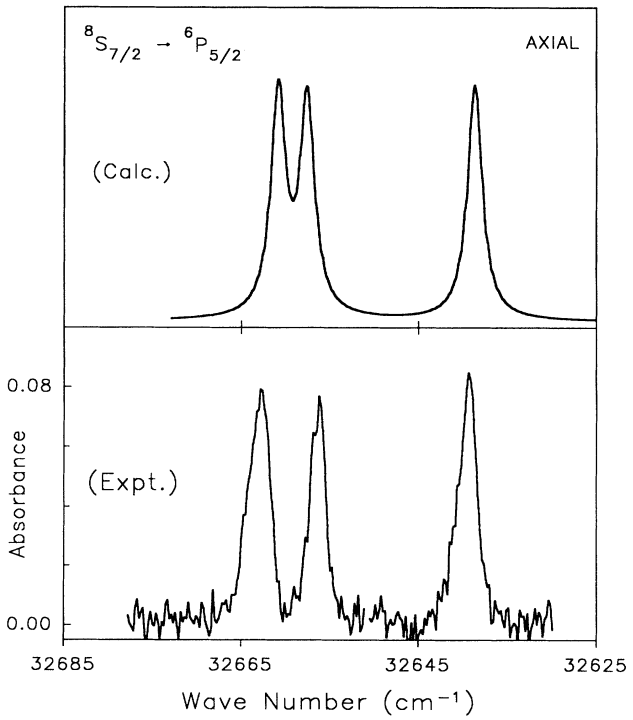

FIG. 2. Experimental and calculated absorption spectra in the $^8S_{7/2} \rightarrow {}^6P_{5.2}$ transition region. Crystal thickness, 0.175 cm; simulation linewidth parameter, $\Delta_t = 2$ cm^{-1}.

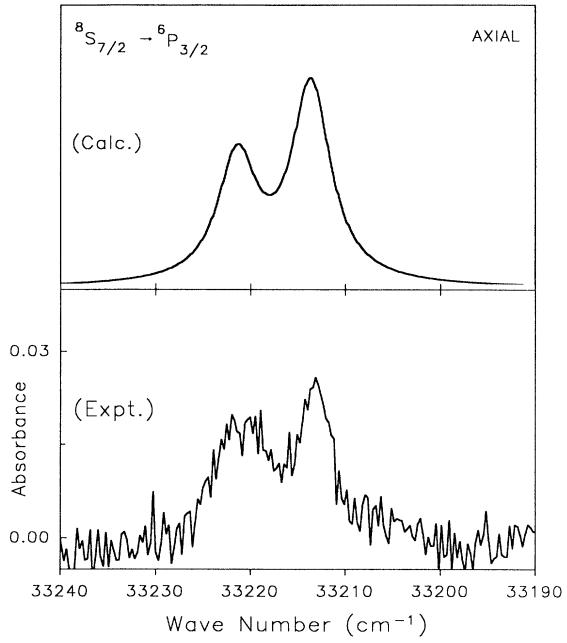

FIG. 3. Experimental and calculated absorption spectra in the $^8S_{7/2} \rightarrow {}^6P_{3/2}$ transition region. Crystal thickness, 0.380 cm; simulation linewidth parameter, $\Delta_t = 5\ cm^{-1}$.

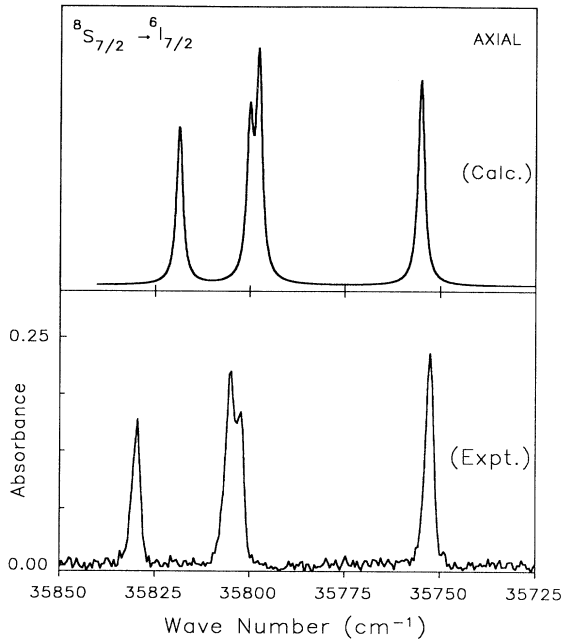

FIG. 4. Experimental and calculated absorption spectra in the $^8S_{7/2} \rightarrow {}^6I_{7/2}$ transition region. Crystal thickness, 0.175 cm; simulation linewidth parameter, $\Delta_t = 2\ cm^{-1}$.

TABLE III. Major-component analysis of $4f^7[SL]J$ state vectors (based on the Hamiltonian parameters listed in Table II).

Multiplet	Energy (cm^{-1})		
label[a]	Calc.[b]	Expt.[c]	Major SL(term) components[d]
$^8S_{7/2}$	1	0	$0.99\,^8S + 0.17\,^6P$
$^6P_{7/2}$	32 054	32 046	$-0.87\,^6P + 0.36\,^6D - 0.20\,^4D(6) - 0.19\,^4D(1) + 0.16\,^8S$
$^6P_{5/2}$	32 630	32 643	$0.91\,^6P - 0.37\,^6D - 0.11\,^4D(6) + 0.10\,^4D(1)$
$^6P_{3/2}$	33 209	33 209	$-0.95\,^6P + 0.28\,^6D + 0.11\,^4S(2)$
$^6I_{7/2}$	35 783	35 781	$-0.96\,^6I - 0.20\,^4H(2) - 0.17\,^4H(3)$
$^6I_{9/2}$	36 122	36 120	$-0.97\,^6I - 0.16\,^4H(2) - 0.14\,^4H(3)$
$^6I_{17/2}$	36 184	36 181	$0.98\,^6I - 0.15\,^4K(1) - 0.13\,^4K(2)$
$^6I_{11/2}$	36 398	36 399	$0.98\,^6I + 0.13\,^4H(2) + 0.10\,^4H(3)$
$^6I_{15/2}$	36 519		$-0.99\,^6I + 0.11\,^4K(1)$
$^6I_{13/2}$	36 555		$0.98\,^6I$
$^6D_{9/2}$	39 504	39 509	$0.96\,^6D - 0.20\,^6F + 0.18\,^4F(4)$
$^6D_{1/2}$	40 428	40 428	$0.99\,^6D$
$^6D_{7/2}$	40 538	40 535	$-0.88\,^6D - 0.36\,^6P + 0.21\,^6F + 0.12\,^4D(3)$
$^6D_{3/2}$	40 701	40 700	$0.94\,^6D + 0.28\,^6P - 0.13\,^6F$
$^6D_{5/2}$	40 840	40 837	$-0.89\,^6D - 0.38\,^6P + 0.18\,^6F + 0.12\,^4D(3)$
$^6G_{7/2}$	48 972		$0.71\,^6G - 0.39\,^6F + 0.26\,^4F(4) - 0.19\,^6H$ $-0.19\,^6D - 0.18\,^4D(6) - 0.17\,^4D(1) + 0.14\,^4G(7)$ $+0.12\,^2F(6) + 0.11\,^4G(1) + 0.11\,^4H(2)$
$^6G_{9/2}$	49 352		$0.79\,^6G - 0.48\,^6F - 0.21\,^6H - 0.19\,^6D$
$^6G_{11/2}$	49 408		$-0.78\,^6G + 0.54\,^6F + 0.20\,^6H + 0.14\,^4G(6) - 0.12\,^4H(2)$
$^6G_{5/2}$	49 430		$-0.76\,^6G + 0.41\,^6F - 0.30\,^4F(4) + 0.19\,^4D(6)$ $+0.18\,^4D(1) + 0.16\,^6H + 0.14\,^6D - 0.11\,^4G(7)$
$^6G_{3/2}$	50 199		$-0.81\,^6G + 0.41\,^6F - 0.30\,^4F(4) + 0.18\,^4D(6) + 0.18\,^4D(1)$
$^6G_{13/2}$	51 012		$-0.94\,^6G + 0.22\,^6H - 0.22\,^4H(2)$

[a]Reflects the *principal SLJ* components of the state vector.
[b]Calculated eigenenergies of $[SL]J$ multiplets.
[c]Multiplet baricenter energies determined from experimental data, with $1/\lambda$(air) to $1/\lambda$(vacuum) corrections included.
[d]Eigenvectors expressed in SL(term) basis.

features. Room-temperature and 10-K transmission spectra in the $^8S_{7/2} \rightarrow {}^6P_{7/2}$ and $^8S_{7/2} \rightarrow {}^6P_{5/2}$ transition regions are compared in Fig. 12.

C. Oscillator strengths

The axial oscillator strengths in the spectra simulations (shown in Figs. 1–9) are listed in Table VII. These oscillator strengths were calculated according to Eq. (10), with $g_A = 8$ and the values of χ'_α, χ_α, and A^λ_{tp} taken from Ref. 33 (which deals with $4f$-$4f$ transition intensities in EuODA). Also listed in Table VII are *isotropic* oscillator strengths calculated according to

$$f_{AB}(\text{isotropic}) = (8\pi m_e c/he^2)\bar{\nu}_{AB}(1/3g_A) \times [\chi' D^{(m)}_{AB} + \chi D^{(e)}_{AB}] , \quad (13)$$

where $D^{(e)}_{AB}$ and $D^{(m)}_{AB}$ are the electric- and magnetic-dipole strengths defined by Eqs. (4) and (5), respectively, and in our calculations we assumed that χ' and χ do not differ significantly from χ'_α and χ_α. The percentage magnetic-dipole contributions to calculated oscillator strengths are shown in separate columns of Table VII. Note that the oscillator strengths calculated within the $^8S_{7/2} \rightarrow {}^6P_{7/2}$ and $^8S_{7/2} \rightarrow {}^6P_{5/2}$ transition manifolds are dominated by magnetic-dipole contributions.

TABLE IV. Calculated and observed baricenters and crystal-field-splitting energies for selected J-multiplet manifolds.

	Baricenter energy (cm^{-1})		Crystal-field-splitting energies (cm^{-1})[a]		
Multiplet	Calculated[b]	Observed[c]	Level[d]	Calculated[b]	Observed[c]
$^6P_{7/2}$	32 054	32 046	5	−14	−10(−8)
		(32 096)	6	0	−2(−2)
			7	4	2(3)
			8	11	10(5)
$^6P_{5/2}$	32 630	32 643	9	−14	−13(−10)
		(32 691)	10	5	4(4)
			11	8	10(6)
$^6P_{3/2}$	33 209	33 209	12	−4	−4(−6)
		(33 254)	13	4	4(6)
$^6I_{7/2}$	35 783	35 781	14	−38	−45(−41)
		(35 805)	15	5	5(3)
			16	7	8(5)
			17	26	32(33)
$^6I_{9/2}$	36 122	36 120	18	−29	−31
			19	−18	−16
			20	6	4
			21	16	18
			22	25	26
$^6I_{11/2}$	36 398	36 399	32	−29	−30(−29)
		(36 442)	33	−16	−15(−16)
			34	−14	−13(−15)
			35	12	7(9)
			36	21	21(26)
			37	28	28(28)
$^6D_{9/2}$	39 504	39 509	53	−53	−52(−52)
		(39 616)	54	−36	−33(−32)
			55	−13	−11(−12)
			56	40	35(38)
			57	60	63(58)
$^6D_{7/2}$	40 538	40 535	59	−7	−6(−7)
		(40 590)	60	−5	−4(−4)
			61	3	2(3)
			62	10	8(8)
$^6D_{5/2}$	40 840	40 837	65	−46	−39(−35)
		(40 905)	66	17	16(13)
			67	28	24(23)

[a]Shown as displacements from the multiplet baricenter.
[b]Calculated using the Hamiltonian parameters listed in Table II of this paper.
[c]Numbers shown in parentheses are from Table I of Ref. 42.
[d]Crystal-field levels numbered as in Table I of this paper.

TABLE V. Comparison of atomic Hamiltonian parameters for Gd^{3+} in GdODA, $LaCl_3$, and LaF_3.

Parameter[a]	GdODA[b]	Values/cm^{-1} Gd^{3+}:LaF_3[c]	Gd^{3+}:$LaCl_3$[d]
F^2	84 138	85 669	84 930
F^4	61 637	60 825	60 209
F^6	44 633	44 776	44 685
α	20.6	18.9	18.3
β	[−600]	[−600]	−639
γ	[1500]	[1575]	1741
T^2	[300]	[300]	[315]
T^3	[42]	[42]	[44]
T^4	[62]	[62]	[40]
T^6	[−295]	[−295]	[−300]
T^7	[350]	[350]	[325]
T^8	[310]	[310]	[360]
$\zeta_{s.o.}$	1499	1508	1500
M^0	3.32	3.22	2.75
P^2	604	676	407
F^4/F^2	0.733	0.710	0.709
F^6/F^2	0.530	0.523	0.526
F^6/F^4	0.724	0.736	0.742

[a]See Eq. (2) in text.
[b]From Table II of this paper.
[c]From Reference 53.
[d]From Reference 61.

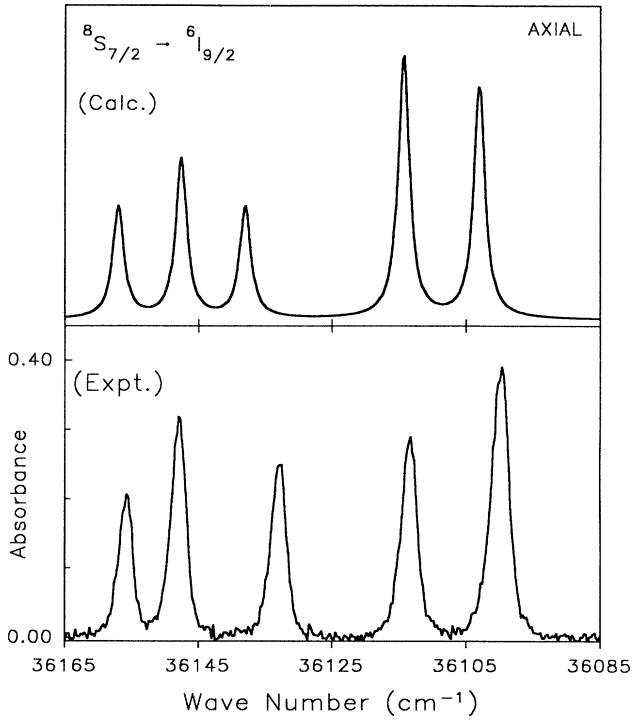

FIG. 5. Experimental and calculated absorption spectra in the $^8S_{7/2} \rightarrow {}^6I_{9/2}$ transition region. Crystal thickness, 0.175 cm; simulation linewidth parameter, $\Delta_t = 2$ cm^{-1}.

V. DISCUSSION

The low-temperature-absorption spectra obtained in this study permit a reasonably complete characterization of crystal-field energy-level structure within the $^6P_J(J=7/2,\ 5/2,$ and $3/2)$, $^6I_J(J=7/2,\ 9/2,\ 17/2,\ 11/2,\ 15/2,$ and $13/2)$, and $^6D_J(J=9/2,\ 1/2,\ 7/2,\ 3/2,$ and $5/2)$ multiplets of the Gd^{3+} $4f^7$ electronic configuration in $Na_3[Gd(ODA)_3]\cdot 2NaClO_4\cdot 6H_2O$. The observed energy-level structure can be accounted for in terms of a parametrized model Hamiltonian that reflects effective D_3 site symmetry at the Gd^{3+} ions, and parametric fits of calculated- to empirical-energy-level data yield values for the Hamiltonian parameters that are compatible with re-

TABLE VI. Comparison of crystal-field energy parameters for Nd^{3+}, Sm^{3+}, Eu^{3+}, Gd^{3+}, Ho^{3+}, and Er^{3+} in $Na_3[M(ODA)_3]\cdot 2NaClO_4\cdot 6H_2O$.

Parameter	NdODA[a]	SmODA[b]	EuODA[c]	GdODA[d]	HoODA[e]	ErODA[f]
			Values/cm^{-1}			
B_{20}	56	−19	−91	−87	−88	−89
B_{40}	−1111	−941	−947	−952	−836	−881
B_{43}	−943	−837	−781	−845	−578	−745
B_{60}	577	606	411	803	531	374
B_{63}	1358	1112	1035	1197	777	661
B_{66}	886	794	755	961	672	648
N	116	144	61	60	105	65
σ/cm^{-1}	14.4	12.3	9.9	6.3	9.1	9.6

[a]From Reference 39.
[b]From Reference 28.
[c]From Refs. 33 and 74.
[d]From Table II of this paper.
[e]From Reference 43.
[f]From Refs. 51 and 74.

TABLE VII. Axial and isotropic oscillator strengths calculated for transitions from the $^8S_{7/2}$ (ground) multiplet manifold to crystal-field levels of the ^6P_J, ^6I_J, and ^6D_J multiplet manifolds. See Sec. III B of the text for a description of the calculations.

Excited level[a]				Oscillator strengths ($\times 10^9$)			
No.	Multiplet	$\|2M_J\|$	$\bar{\nu}$(cm^{-1})[b]	axial[c]	%MD[d]	isotropic[e]	%MD[d]
5	$^6P_{7/2}$	1	32 045	16.5	83.7	16.0	88.7
6	$^6P_{7/2}$	7	32 053	12.1	80.6	15.8	89.8
7	$^6P_{7/2}$	3	32 057	22.0	83.0	16.8	84.9
8	$^6P_{7/2}$	5	32 066	18.4	82.6	16.3	86.6
9	$^6P_{5/2}$	5	32 640	12.4	97.0	10.8	97.7
10	$^6P_{5/2}$	1	32 656	11.5	83.4	11.9	89.1
11	$^6P_{5/2}$	3	32 663	11.8	86.6	11.8	91.0
12	$^6P_{3/2}$	1	33 214	1.0	0.14	0.7	0.1
13	$^6P_{3/2}$	3	33 222	0.7	1.4	0.4	1.6
14	$^6I_{7/2}$	1	35 747	32.9	<0.1	50.4	<0.1
15	$^6I_{7/2}$	7	35 796	33.7	0.2	24.4	0.2
16	$^6I_{7/2}$	3	35 799	23.5	0.2	15.8	0.3
17	$^6I_{7/2}$	5	35 824	25.4	0.2	45.7	0.1
18	$^6I_{9/2}$	1	36 100	81.3	<0.1	110	<0.1
19	$^6I_{9/2}$	9	36 114	93.8	<0.1	100	<0.1
20	$^6I_{9/2}$	3	36 134	39.6	<0.1	45.5	<0.1
21	$^6I_{9/2}$	5	36 149	55.9	<0.1	50.3	<0.1
22	$^6I_{9/2}$	7	36 156	39.1	<0.1	90.1	<0.1
23	$^6I_{17/2}$	11	36 173	57.8	<0.1	67.5	<0.1
24	$^6I_{17/2}$	9	36 174	101	<0.1	79.8	<0.1
25	$^6I_{17/2}$	7	36 175	65.7	<0.1	120	<0.1
26	$^6I_{17/2}$	15	36 187	88.8	<0.1	87.2	<0.1
27	$^6I_{17/2}$	1	36 187	23.5	0.1	19.5	0.2
28	$^6I_{17/2}$	5	36 192	66.2	0.1	78.2	<0.1
29	$^6I_{17/2}$	7		63.8	<0.1	114	<0.1
30	$^6I_{17/2}$	9	36 213	119	<0.1	85.0	<0.1
31	$^6I_{17/2}$	17	36 214	17.9	0.40	15.2	0.3
32	$^6I_{11/2}$	1	36 379	93.4	<0.1	116	<0.1
33	$^6I_{11/2}$	11	36 394	149	<0.1	133	<0.1
34	$^6I_{11/2}$	3	36 397	70.3	<0.1	93.1	<0.1
35	$^6I_{11/2}$	5	36 417	38.1	<0.1	56.9	<0.1
36	$^6I_{11/2}$	9	36 430	61.4	<0.1	98.0	<0.1
37	$^6I_{11/2}$	7	36 438	88.0	<0.1	101	<0.1
38	$^6I_{15/2}$	1	36 496	52.1	<0.1	101	<0.1
39	$^6I_{15/2}$	3	36 506	63.6	<0.1	103	<0.1
40	$^6I_{15/2}$	11		84.5	<0.1	123	<0.1
41	$^6I_{15/2}$	15		104	<0.1	78.8	<0.1
42	$^6I_{15/2}$	13	36 520	227	<0.1	233	<0.1
43	$^6I_{13/2}$	1	36 530	78.4	<0.1	127	<0.1
44	$^6I_{13/2}$	13	36 540	149	<0.1	107	<0.1
45	$^6I_{13/2}$	3		122	<0.1	83.8	<0.1
46	$^6I_{15/2}$	7	36 555	40.8	<0.1	61.6	<0.1
47	$^6I_{13/2}$	11	36 564	81.0	<0.1	36.1	<0.1
48	$^6I_{15/2}$	9	36 569	32.8	0.11	56.3	<0.1
49	$^6I_{15/2}$	5	36 572	53.5	<0.1	53.4	<0.1
50	$^6I_{13/2}$	7	36 597	21.9	<0.1	56.0	<0.1
51	$^6I_{13/2}$	5	36 601	73.6	<0.1	75.8	<0.1
52	$^6I_{13/2}$	9	36 608	102	<0.1	73.3	<0.1
53	$^6D_{9/2}$	7	39 469	12.7	0.7	8.7	1.1
54	$^6D_{9/2}$	5	39 488	18.5	0.5	12.3	0.8
55	$^6D_{9/2}$	3	39 510	12.2	0.8	8.4	1.1
56	$^6D_{9/2}$	9	39 556	27.3	0.5	17.9	0.5
57	$^6D_{9/2}$	1	39 583	22.1	0.3	14.6	0.7
58	$^6D_{1/2}$	1	40 440	1.3	6.1	0.9	7.9
59	$^6D_{7/2}$	7	40 541	1.1	9.9	8.3	18.1
60	$^6D_{7/2}$	3	40 543	20.8	8.4	14.1	10.1
61	$^6D_{7/2}$	1	40 549	23.7	6.8	15.9	9.0

TABLE VII. (*Continued*).

Excited level[a]				Oscillator strengths ($\times 10^9$)			
No.	Multiplet	$\|2M_J\|$	$\bar{\nu}$(cm^{-1})[b]	axial[c]	%MD[d]	isotropic[e]	%MD[d]
62	$^6D_{7/2}$	5	40555	21.6	6.2	15.1	9.6
63	$^6D_{3/2}$	3		11.9	1.2	8.0	1.3
64	$^6D_{3/2}$	1	40712	4.0	1.8	2.7	3.8
65	$^6D_{5/2}$	1	40810	13.9	7.7	9.7	1.1
66	$^6D_{5/2}$	5	40865	10.2	10.0	7.1	14.4
67	$^6D_{5/2}$	3	40874	17.6	5.8	12.4	8.3

[a]Identified according to the labels given in Table I.
[b]Transition energy expressed in the wavenumber units, $1/\lambda$(air).
[c]Calculated according to Eq. (9) of the text.
[d]Percent (%) magnetic-dipole (MD) contribution to calculated oscillator strength.
[e]Calculated according to Eq. (13) of the text.

sults reported previously for Gd^{3+} in other crystalline hosts (see Table V) *and* for other lanthanide ions in $Na_3[M(ODA)_3]\cdot 2NaClO_4\cdot 6H_2O$ systems (see Table VI). Calculated *versus* experimentally-observed crystal-field-splittings within J-multiplet manifolds generally agree to within the uncertainty limits of the experimental measurements, and calculated *versus* observed J-multiplet baricenter energies differ by less than 5 cm^{-1} for all multiplets except $^6P_{7/2}$ and $^6P_{5/2}$ (where the differences are 8 and 13 cm^{-1}, respectively; see Tables III and IV). Furthermore, the absorption intensity distributions observed both *within* and *among* the various $^8S_{7/2}\rightarrow{}^6P_J$, ^6I_J, and ^6D_J multiplet-to-multiplet transition manifolds are reproduced with good fidelity by calculations based on a model that was developed in previous studies of lanthanide $4f$-$4f$ transition intensities.

The quantitative data analyses reported in this study were based on absorption measurements carried out on samples at low temperature (approximately 10 K). Variable-temperature measurements carried out between 10 and 298 K showed only very small changes in J-multiplet baricenter energies, crystal-field-splitting ener-

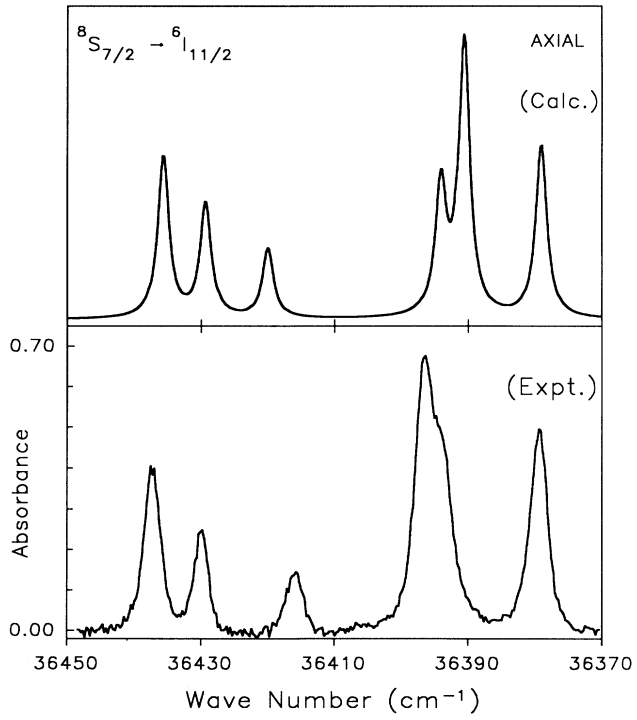

FIG. 6. Experimental and calculated absorption spectra in the $^8S_{7/2}\rightarrow{}^6I_{11/2}$ transition region. Crystal thickness, 0.175 cm; simulation linewidth parameter, $\Delta_t = 2$ cm^{-1}.

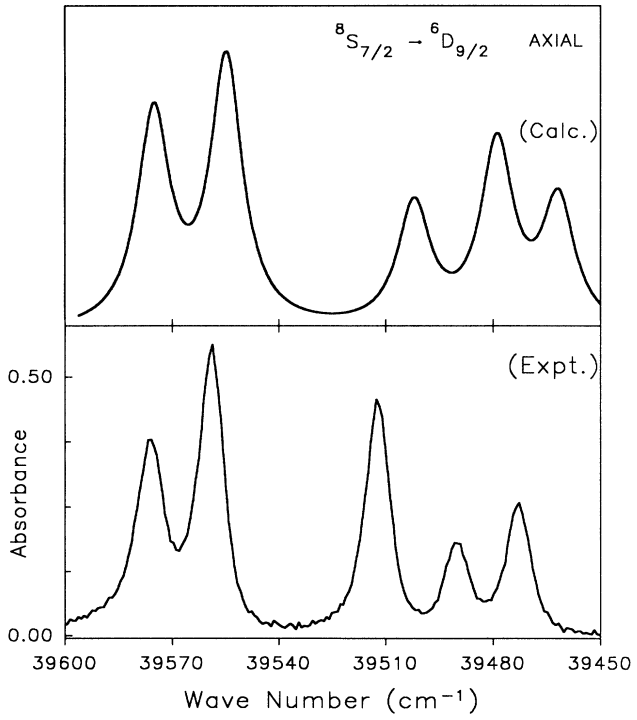

FIG. 7. Experimental and calculated absorption spectra in the $^8S_{7/2}\rightarrow{}^6D_{9/2}$ transition region. Crystal thickness, 0.380 cm; simulation linewidth parameter, $\Delta_t = 11$ cm^{-1}.

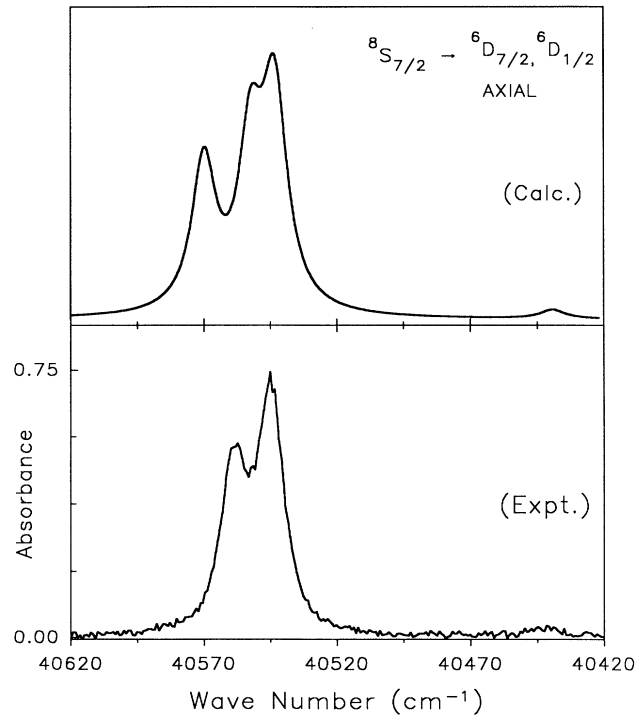

FIG. 8. Experimental and calculated absorption spectra in the $^8S_{7/2} \rightarrow {}^6D_{7/2}$, $^6D_{1/2}$ transition region. Crystal thickness, 0.380 cm; simulation linewidth parameter, $\Delta_t = 11$ cm^{-1}.

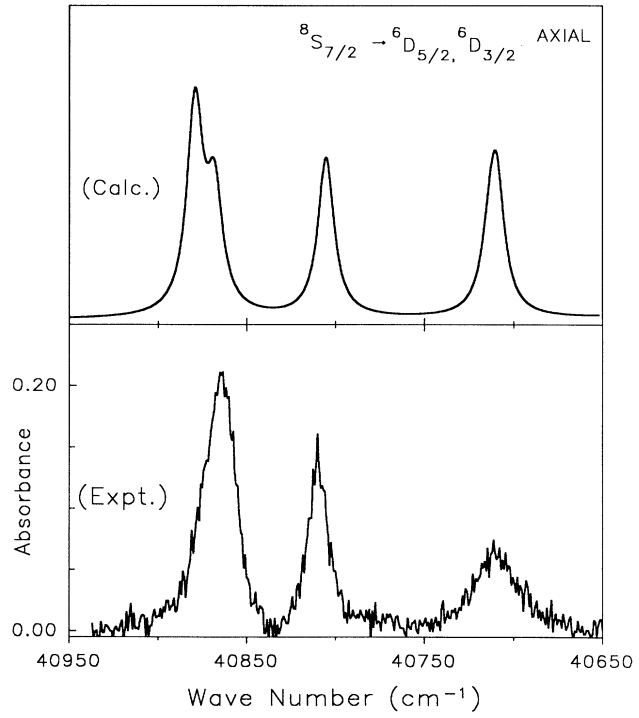

FIG. 9. Experimental and calculated absorption spectra in the $^8S_{7/2} \rightarrow {}^6D_{5/2}$, $^6D_{3/2}$ transition region. Crystal thickness, 0.380 cm; simulation linewidth parameter, $\Delta_t = 11$ cm^{-1}.

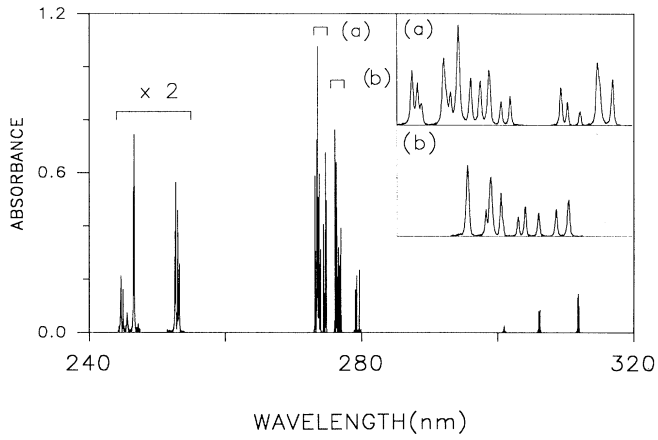

FIG. 10. Survey absorption spectrum, and insets showing spectral details within the $^8S_{7/2} \rightarrow {}^6I_J(J = 13/2, 15/2, 11/2)$ [inset (a)] and $^8S_{7/2} \rightarrow {}^6I_J(J = 17/2, 9/2)$ [inset (b)] transition regions. Each inset spans a 2-nm wavelength range.

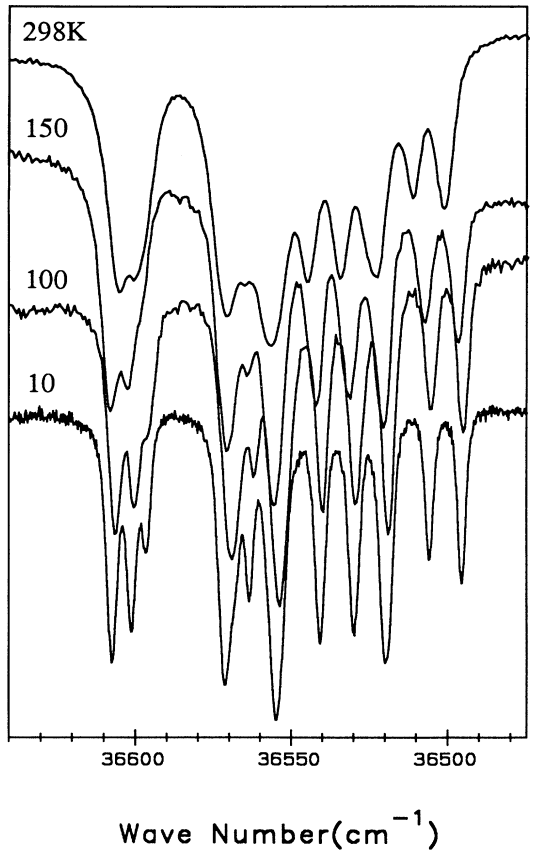

FIG. 11. Transmission spectra recorded in the $^8S_{7/2} \rightarrow {}^6I_J(J = 13/2$ and $15/2)$ transition region at sample temperatures of 298, 150, 100 and 10 K.

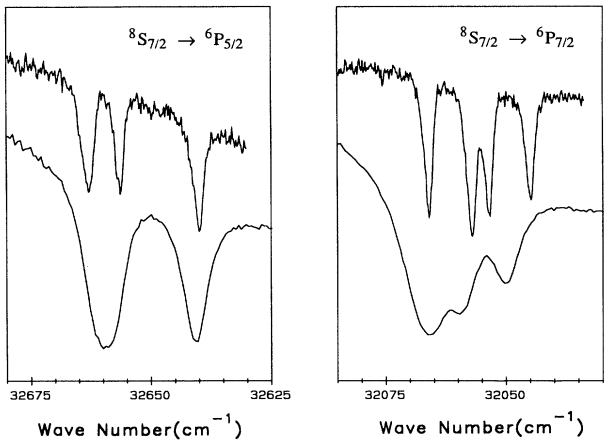

FIG. 12. Transmission spectra recorded in the $^8S_{7/2} \rightarrow {}^6P_{7/2}$ and $^8S_{7/2} \rightarrow {}^6P_{5/2}$ transition regions at sample temperatures of 298 K (lower traces) and 10 K (upper traces).

gies, and transition intensity distributions. Neither our room-temperature absorption results nor our parametric analyses of the low-temperature absorption data yield energy-level structures that are compatible with the energy-level scheme and parametric Hamiltonian reported in Ref. 42 (although, as is shown in Table IV, the crystal-field-splitting energies reported here and in Ref. 42 are in reasonably good agreement). This is troublesome because the two-photon luminescence excitation experiments reported in Ref. 42 have significant potential for advancing our understanding of two-photon-induced $4f$-$4f$ transition processes in noncentrosymmetric lanthanide systems. However, a satisfactory analysis of two-photon intensity data must be predicated on a reasonably detailed and accurate knowledge of energy-level structure (including state-vector characterizations).[68–72]

It is possible that the disparities between the energy-level results reported here and in Ref. 42 can be traced to wavelength calibration problems in the dye lasers used for the two-photon luminescence excitation measurements. This type of calibration error would be manifested most prominently in the observed locations of multiplet-to-multiplet transition baricenters, and they would be less apparent (and perhaps not observed at all) in the splittings between crystal-field components *within* multiplet-to-multiplet transition manifolds. It is also possible, though unlikely, that the one-photon-absorption measurements (reported here) and the two-photon excitation measurements (reported in Ref. 42) probe different energy levels of Gd^{3+} in $Na_3[Gd(ODA)_3] \cdot 2NaClO_4 \cdot 6H_2O$. The transition frequencies reported in Ref. 42 are, on average, approximately 50 cm^{-1} *higher* than those observed in our measurements. This might suggest that the two-photon-absorption cross sections peak on excited *vibronic* levels, displaced from the zero-phonon (vibrationless) electronic levels by ≈ 50 cm^{-1}. However, this suggestion is highly speculative, and it has no obvious justification within the framework of current two-photon-absorption intensity theory.

Eigenvalues of the parametrized model Hamiltonian developed in this study give a good account of the Gd^{3+} $4f^7$ energy-level structure up to 41 000 cm^{-1}, and the eigenvectors of this Hamiltonian proved useful in calculations of one-photon-absorption intensities throughout the $^8S_{7/2} \rightarrow {}^6P_J$, ^6I_J, and ^6D_J multiplet-to-multiplet transition regions (from 32 000 to 41 000 cm^{-1}). It is likely that the energy eigenvalues and $4f^7$ electronic state vectors derived from the analyses reported here will be of considerable utility in further analyses of the two-photon excitation results reported in Ref. 42. Additionally, the electronic state structure characterized in the present study should provide a satisfactory basis for interpreting the very complex circular dichroism spectra exhibited by Gd^{3+} in trigonal $Na_3[Gd(ODA)_3] \cdot 2NaClO_4 \cdot 6H_2O$ (Refs. 16 and 73). Lanthanide $4f$-$4f$ circular dichroism spectra are extraordinarily sensitive to the details of $4f^N$ electronic state structure, and they provide an excellent probe of $SLJM_J$ state-vector compositions (Refs. 25, 26, 30, 34, 38, 41, and 50).

ACKNOWLEDGMENTS

This work was supported by the U.S. National Science Foundation (NSF Grant No. CHE-8820180 to F.S.R.) and by the U.S. National Institutes of Health (NIH Grant No. DK35865 to E.M.S.). The authors also gratefully acknowledge much useful advice and help from Dr. Michael F. Reid.

*Author to whom correspondence should be addressed.

[1]B. Norden and I. Grenthe, Acta. Chem. Scand. **26**, 407 (1972).
[2]A. C. Sen, S. C. Bera, and M. Chowdhury, Chem. Phys. Lett. **46**, 594 (1977).
[3]A. K. Banerjee, R. K. Mukherjee, and M. Chowdhury, J. Chem. Soc. Faraday Trans. 2 **75**, 337 (1979).
[4]R. W. Schwartz, A. K. Banerjee, A. C. Sen, and M. Chowdhury, J. Chem. Soc. Faraday Trans. 2 **76**, 620 (1980).
[5]A. K. Banerjee, A. C. Sen, and M. Chowdhury, Chem. Phys. Lett. **69**, 592 (1980).
[6]R. Kuroda, S. F. Mason, and C. Rosini, Chem. Phys. Lett. **70**, 11 (1980).
[7]R. Kuroda, S. F. Mason, and C. Rosini, J. Chem. Soc. Faraday Trans. 2 **77**, 2125 (1981).
[8]A. C. Sen, M. Chowdhury, and R. W. Schwartz, J. Chem. Soc. Faraday Trans. 2 **77**, 1293 (1981).
[9]A. K. Banerjee, R. W. Schwartz, and M. Chowdhury, J. Chem. Soc. Faraday Trans. 2 **77**, 1635 (1981).
[10]D. S. Roy, K. Bhattacharyya, A. K. Gupta, and M. Chowdhury, Chem. Phys. Lett. **77**, 422 (1981).
[11]R. W. Schwartz, A. K. Banerjee, M. Chowdhury, and R. Kuroda, J. Chem. Soc. Faraday Trans. 2 **77**, 557 (1981).
[12]A. C. Sen and M. Chowdhury, Chem. Phys. Lett. **79**, 165 (1981).

[13]F. S. Richardson, J. D. Saxe, S. A. Davis, and T. R. Faulkner, Mol. Phys. **42**, 1401 (1981).
[14]J. P. Morley, J. D. Saxe, and F. S. Richardson, Mol. Phys. **47**, 379 (1982).
[15]J. D. Saxe, J. P. Morley, and F. S. Richardson, Mol. Phys. **47**, 407 (1982).
[16]P. K. Chatterjee and M. Chowdhury, J. Chem. Soc. Faraday Trans. 2 **78**, 429 (1982).
[17]F. S. Richardson and T. R. Faulkner, J. Chem. Phys. **76**, 1595 (1982).
[18]J. D. Saxe, T. R. Faulkner, and F. S. Richardson, J. Chem. Phys. **76**, 1607 (1982).
[19]A. K. Banerjee and R. W. Schwartz, J. Chem. Soc. Faraday Trans. 2 **79**, 755 (1983).
[20]A. F. Kirby and F. S. Richardson, J. Phys. Chem. **87**, 2557 (1983).
[21]B. Karmakar, D. S. Roy, K. Bhattacharyya, A. Samanta, and M. Chowdhury, Chem. Phys. Lett. **97**, 545 (1983).
[22]J. J. Dallara, M. F. Reid, and F. S. Richardson, J. Phys. Chem. **88**, 3587 (1984).
[23]B. Karmakar, P. K. Chatterjee, D. S. Roy, D. Nath, M. Chowdhury, and B. Walklyn, Chem. Phys. Lett. **107**, 203 (1984).
[24]M. Albin, R. R. Whittle, and W. DeW. Horrocks, Jr., Inorg. Chem. **24**, 4591 (1985).
[25]F. S. Richardson, M. T. Berry, and M. F. Reid, Mol. Phys. **58**, 929 (1986).
[26]M. T. Berry and F. S. Richardson, J. Less-Common Met. **126**, 251 (1986).
[27]R. C. Carter, C. E. Miller, R. A. Palmer, P. S. May, D. H. Metcalf, and F. S. Richardson, Chem. Phys. Lett. **131**, 37 (1986).
[28]P. S. May, M. F. Reid, and F. S. Richardson, Mol. Phys. **61**, 1455 (1987).
[29]P. S. May, M. F. Reid, and F. S. Richardson, Mol. Phys. **61**, 1471 (1987).
[30]P. S. May, M. F. Reid, and F. S. Richardson, Mol. Phys. **62**, 341 (1987).
[31]M. Vala, D. Nath, M. Chowdhury, A. Wierzbicki, and A. C. Sen, Chem. Phys. Lett. **134**, 610 (1987).
[32]B. Karmakar, P. K. Chatterjee, S. Basu, and M. Chowdhury, Bull. Chem. Soc. Jpn. **60**, 2993 (1987).
[33]M. T. Berry, C. Schwieters, and F. S. Richardson, Chem. Phys. **122**, 105 (1988).
[34]M. T. Berry, C. Schwieters, and F. S. Richardson, Chem. Phys. **122**, 125 (1988).
[35]M. Vala, J. Szczepanski, A. K. Banerjee, and M. Chowdhury, Chem. Phys. **134**, 149 (1989).
[36]K. A. Schoene and F. S. Richardson, J. Less-Common Met. **148**, 305 (1989).
[37]D. H. Metcalf and F. S. Richardson, J. Less-Common Met. **148**, 321 (1989).
[38]D. M. Moran, A. DePiante, and F. S. Richardson, J. Less-Common Met. **148**, 297 (1989).
[39]P. S. May, C. K. Jayasankar, and F. S. Richardson, Chem. Phys. **138**, 123 (1989).
[40]P. S. May, C. K. Jayasankar, and F. S. Richardson, Chem. Phys. **138**, 139 (1989).
[41]F. S. Richardson, J. Less-Common Met. **149**, 161 (1989).
[42]T. Kundu, A. K. Banerjee, and M. Chowdhury, Phys. Rev. B **41**, 10 911 (1990).
[43]D. M. Moran, A. De Piante, and F. S. Richardson, Phys. Rev. B **42**, 3317 (1990).
[44]D. M. Moran and F. S. Richardson, Phys. Rev. B **42**, 3331 (1990).
[45]S. Dasgupta, M. Saha, and G. Ghosh, J. Phys. C **19**, 1771 (1986).
[46]J. Albertsson, Acta Chem. Scand. **22**, 1563 (1968).
[47]J. Albertsson, Acta Chem. Scand. **24**, 3527 (1970).
[48]J. Albertsson and I. Elding, Acta Chem. Scand. Ser. A **31**, 21 (1977).
[49]F. R. Fronczek, A. K. Banerjee, S. F. Watkins, and R. W. Schwartz, Inorg. Chem. **20**, 2745 (1981).
[50]P. S. May, Ph.D. dissertation, University of Virginia, 1988.
[51]K. A. Schoene, Ph.D. dissertation, University of Virginia, 1989.
[52]H. M. Crosswhite and H. Crosswhite, J. Opt. Soc. Am. B **1**, 246 (1984).
[53]W. T. Carnall, G. L. Goodman, K. Rajnak, and R. S. Rana, J. Chem. Phys. **90**, 3443 (1989).
[54]M. F. Reid, J. Chem. Phys. **87**, 2875 (1987).
[55]M. F. Reid and F. S. Richardson, J. Chem. Phys. **83**, 3831 (1985).
[56]H. Crosswhite and D. J. Newman, J. Chem. Phys. **81**, 4959 (1984).
[57]Y. Y. Yeung and D. J. Newman, J. Phys. C **19**, 3877 (1986).
[58]Y. Y. Yeung and D. J. Newman, J. Chem. Phys. **86**, 6717 (1987).
[59]M. F. Reid, F. S. Richardson, and P. A. Tanner, Mol. Phys. **60**, 881 (1987).
[60]C. K. Jayasankar, F. S. Richardson, P. A. Tanner, and M. F. Reid, Mol. Phys. **61**, 635 (1987).
[61]C. K. Jayasankar, M. F. Reid, and F. S. Richardson, J. Less-Common Met. **148**, 289 (1989).
[62]C. K. Jayasankar, M. F. Reid, and F. S. Richardson, Phys. Status Solidi B **155**, 559 (1989).
[63]M. F. Reid and F. S. Richardson, J. Chem. Phys. **79**, 5735 (1983).
[64]M. F. Reid and F. S. Richardson, J. Phys. Chem. **88**, 3579 (1984).
[65]B. R. Judd, Phys. Rev. **127**, 750 (1962).
[66]G. S. Ofelt, J. Chem. Phys. **37**, 511 (1962).
[67]J. D. Axe, J. Chem. Phys. **39**, 1154 (1963).
[68]M. C. Downer and A. Bivas, Phys. Rev. B **28**, 3677 (1983).
[69]B. R. Judd and D. R. Pooler, J. Phys. C **15**, 591 (1982).
[70]M. F. Reid and F. S. Richardson, Phys. Rev. B **29**, 2830 (1984).
[71]J. Sztucki and W. Strek, Phys. Rev. B **34**, 3120 (1986).
[72]L. Smentek-Mielczarek and B. A. Hess, Phys. Rev. B **36**, 1811 (1987).
[73]E. M. Stephens, D. H. Metcalf, and F. S. Richardson (unpublished results).
[74]J. Quagliano (unpublished results).